Chinese Journal of Aeronautics, (2025), 38(7): 103469

Chinese Society of Aeronautics and Astronautics
& Beihang University

Chinese Journal of Aeronautics

cja@buaa.edu.cn
www.sciencedirect.com

FULL LENGTH ARTICLE

Feasibility of scintillation monitoring with low-cost GNSS receivers using geodetic detrending

Guillermo GONZÁLEZ-CASADO *, Jorge GARCÍA-MATEOS, Yu YIN, Angela ARAGON-ANGEL, José Miguel JUAN, Cristhian C. TIMOTE, Adria ROVIRA-GARCIA, Jaume SANZ

Research Group of Astronomy and Geomatics, Universitat Politècnica de Catalunya Barcelona Tech, Barcelona E-08034, Spain

Received 21 June 2024; revised 3 March 2025; accepted 4 March 2025
Available online 7 March 2025

KEYWORDS

Geodetic detrending;
GNSS signals;
Ionosphere;
Low-cost receivers;
Scintillation

Abstract The geodetic detrending (GD) methodology was introduced in the past decade and has opened the door to the global monitoring of ionospheric scintillation using global navigation satellite system (GNSS) receivers. The performance of GD has been demonstrated in geodetic receivers. However, extending scintillation monitoring to low-cost commercial receivers remains a challenge. Low-cost devices could serve as valuable complements to specialised and much more expensive scintillation monitoring receivers. In this paper, first, a feasibility study was conducted using the GD technique, demonstrating that the scintillation indices derived from the observations of two low-cost receivers (Septentrio Mosaic X5 and UBLOX ZED-F9P) have a resolution similar to that achieved by geodetic receiver models, whose price is one order of magnitude higher. Second, measurements of GNSS signals at different frequencies from the Galileo and global positioning system (GPS) satellites were analysed in a specific experiment over six days of null scintillation. Next, the noise level in the scintillation parameters derived from the experiment was evaluated, which shows that for low-cost receivers, the minimum scintillation detection threshold increases only negligibly compared to geodetic-grade receivers. Moreover, the geometry-free (GF) combination of L1 with a second signal of different frequency was investigated as an alternative to detrending GNSS signals. Finally, for determining the ionospheric fluctuations produced by scintillation, the limitations of using the GF combination versus the uncombined measurements were highlighted. It is concluded that the minimum resolution of scintillation indices derived from low-cost receiver measurements makes it possible to distinguish values associated with periods of scintillation activity from those produced by residual noise from mismodeling. For both geodetic and low-cost receivers, the scin-

* Corresponding author.
E-mail address: guillermo.gonzalez@upc.edu (G. GONZÁLEZ-CASADO).

☆ This article is part of a special issue entitled: 'GNSS Technology and Application' published in Chinese Journal of Aeronautics.
Peer review under responsibility of Editorial Committee of CJA

Production and hosting by Elsevier

https://doi.org/10.1016/j.cja.2025.103469

tillation detection threshold obtained with uncombined carrier-phase measurements is smaller than that achieved with the classic GF combination.

1. Introduction

Ionospheric scintillation refers to the rapid fluctuations in the intensity and phase of radio signals, including those transmitted by global navigation satellite systems (GNSSs). As these signals travel, they encounter irregularities in the electron distribution in the ionosphere, which cause refraction and/or diffraction effects. This disruption negatively affects the performance of communication and navigation systems that rely on satellite signals. Scintillation leads to an increased level of noise in GNSS signals and can even cause receivers to lose a lock on tracking these signals or make them difficult to acquire. Consequently, addressing scintillation has become a significant concern in the field of navigation.[1,2] Correcting or mitigating the effects of scintillation is currently a crucial challenge for achieving precise GNSS navigation.[3,4]

To measure scintillation using GNSS observations, it is first necessary to isolate the high-frequency fluctuations caused by the ionospheric delay experienced by the GNSS signal. This separation can be achieved by applying a high-pass filter (HPF), such as the sixth-order Butterworth filter with a typical cut-off frequency of 0.1 Hz.[5] However, certain effects such as cycle slips (CSs) in the carrier phase measurements or clock jitter may persist, producing high-frequency fluctuations even after the application of an HPF, which must be eliminated or mitigated before HPF application. Various techniques can be employed for this purpose, including the use of open-loop receivers,[6] gathering data at a high frequency ($\geq$ 50 Hz), or synchronising the receiver clock with a highly stable external clock.

Ionospheric scintillation monitoring receivers (ISMRs) are equipped with special firmware designed to process GNSS signals under disturbed ionospheric conditions using the aforementioned techniques. This enables direct monitoring of high-frequency fluctuations in GNSS signals caused by electron density gradients in the ionosphere. ISMRs produce several scintillation indices that can be used to quantify the impact of the scintillation activity on GNSS signals.

The standard deviation of the signal power, normalised by its mean, is defined as the amplitude scintillation index S_4:[5,7]

$$S_4 = \sqrt{\frac{\langle \mathrm{SI}^2 \rangle - \langle \mathrm{SI} \rangle^2}{\langle \mathrm{SI} \rangle^2}} \tag{1}$$

where SI represents the signal intensity. S_4 is generally computed over a period of one minute.

The standard deviation of the detrended carrier phase is defined as the phase scintillation index, σ_φ: [8]

$$\sigma_\varphi = \sqrt{\langle \varphi^2 \rangle - \langle \varphi \rangle^2} \tag{2}$$

where φ denotes the detrended carrier phase measurement after having applied an HPF. This index, which is typically calculated over 1 min, measures the carrier phase fluctuations caused by ionospheric irregularities. Unlike signal amplitude fading, these fluctuations can manifest themselves in the presence of large-scale irregularities.[9]

Juan et al. introduced the geodetic detrending (GD) method.[10] GD involves the accurate modelling of the nondispersive (geodetic) effects of GNSS signals, accounting for satellite and receiver clock fluctuations. This approach also enables the detection of small CSs that commonly occur in measurements obtained using conventional receivers under scintillation conditions. Consequently, GD facilitates the isolation of ionospheric delays and their high-frequency fluctuations in a manner similar to that of ISMRs. Subsequently, the remaining low-frequency components in the signals can be removed using an HPF.[11]

The GD technique applied to geodetic GNSS receivers, such as those used in the International GNSS Service (IGS) network, has been introduced, and its performance has been assessed and validated in several previous studies.[4,10,12,13] Therefore, the objective of this study is to present a feasibility analysis of the performance of low-cost GNSS receivers for scintillation monitoring based on the same GD methodology for the derivation of scintillation indices as in our previous studies, following a similar methodology for performance evaluation.[10,12,13] Low-cost receivers are expected to have higher thermal noise that could be misinterpreted as scintillation. Therefore, the main goal of this study is to establish a minimum threshold for scintillation detection using such devices. This is accomplished by analysing their performance during periods of no scintillation activity and verifying that the values of the reported scintillation indices are low enough not to result in false scintillation detections. In this respect, the minimum threshold constrains the upper range of the values of the corresponding scintillation index in the absence of fast fluctuations in the ionospheric electron density. Therefore, index values above this threshold would only be produced by the presence of rapid fluctuations in the ionosphere, so the threshold is a lower limit of the index values that can be attributed to ionospheric scintillation affecting GNSS signals.

In the present study, the outcomes derived from two low-cost devices, Septentrio Mosaic X5 and UBLOX ZED-F9P, were compared with the results obtained using several geodetic receivers manufactured by Septentrio that are commonly found in IGS networks. These low-cost devices have been previously recommended for GNSS applications.[14,15] Finally, the performance of a low-cost receiver under scintillation is illustrated by presenting an example of the results obtained from a UBLOX receiver located in a low-latitude region.

The comparison between low-cost and geodetic receivers has been focused on the conventional scintillation indices, S_4 and σ_φ, derived from each type of device. However, the geometry-free (GF) combination of two GNSS signals of different frequencies from geodetic receivers is also a common detrending strategy used to monitor ionospheric activity considering the rate of total electron content index (ROTI).[16,17]

Therefore, the present study addresses the limitations of using the GF combination to characterise ionospheric fluctuations,[11,17] highlighting the advantages of an approach based on uncombined carrier phase measurements.

The final objective of the present feasibility study is to develop a cost-effective alternative for assessing ionospheric scintillation and total electron content (TEC) using affordable GNSS receivers. This lays the groundwork for an ionospheric monitoring system that would be characterised by its ease of deployment and operation worldwide, with a significantly reduced cost compared to highly specialised and expensive alternatives, such as ISMRs or high-grade geodetic devices.

2. Methodology

The GD technique has been presented and assessed in previous studies,[10,12] and the same methodology was applied in the present study. Therefore, in this section, the description of the technique is limited to specific aspects of interest for subsequent analysis.

The methodology applied in the GD technique consists of modelling or calculating all non-dispersive effects (i.e., geodetic) as accurately as possible to detrend the carrier-phase measurements from GNSS satellites recorded at intervals of 1 s. For this study, post-processed products for satellite orbit and clock corrections from the IGS were used. Precise products for troposphere delays were also taken from the IGS in the case of measurements from receivers belonging to that network (see Table 1). By contrast, for the receivers located at the Universitat Politècnica de Catalunya (UPC) premises, the vertical zenith path delay and the precise coordinates were calculated by performing precise point positioning processing. For the IGS receivers, precise coordinates and antenna phase centre corrections were obtained from the IGS products in the standard SINEX and ANTEX formats. Relativistic, wind-up, tides, and ocean loading effects were modelled according to standard formulas.[18] Finally, after removing the previous terms from the carrier phase measurements of two different frequencies, the receiver clock offsets per second were calculated following a method based on the use of the ionosphere-free (IF) combination of the detrended carrier phase residuals from the two different GNSS signals processed in the previous step of the GD.[10,12]

Fast fluctuations in the receiver clock must be accurately calculated to remove them from carrier-phase observations. Receiver clock fluctuations can introduce fast variations in the detrended carrier-phase residuals, giving rise to high values of the phase scintillation index that are not related to scintillation or ionosphere variability. GD processing calculates the receiver clock offset at the same sampling time interval as the carrier-phase observations, that is, 1 s in this study. In this respect, the most relevant feature observed in the receivers listed in Table 1 is the existence of regular-leap millisecond corrections that are automatically applied to the internal clock of the Septentrio Mosaic X5 low-cost receiver UPC1 approximately every 25 min and to the UBLOX device UPC3 approximately every 15 min. Despite this, the GD method can properly model the time evolution of the clock offsets. An example of short-timescale fluctuations of the clocks in the receivers listed in Table 1 is shown in Fig. 1. In this figure receiver clock fluctuations (in meters) were obtained from the GD after removing a linear fit to the clock offsets. The offsets were calculated using all satellites in view of each receiver. Results are shown during a time interval of 700 s from day of year (DoY) 195 in 2023. The zoomed-in graph in the bottom left side illustrates in greater detail the magnitude of the fluctuations of the UBLOX clock after the clock steering. As shown in Fig. 1, the clocks from the geodetic receivers may have fluctuations ranging from centimetres to several decimetres in short time periods, whereas the geodetic receiver UPC2 shows only slightly larger fluctuations than the clocks in the IGS receivers KOS1 and DYNG. Conversely, the clock in the Septentrio Mosaic-X5 UPC1 can have fluctuations of several meters on timescales of tens of seconds. This is reasonable because one can expect the quality of the clock from a low-cost device to be poorer than that of higher-grade geodetic receivers. Finally, the UBLOX receiver was configured to use clock steering, and consequently, the resulting clock fluctuations estimated from the GD method were small (see the black line in Fig. 1) but still at the level of a few centimetres, as illustrated in the zoomed-in plot at the bottom left of Fig. 1. Note that, for the σ_φ index from L1/E1 carrier frequency, a value of 1 rad is equal to 3 cm. Therefore, the determination of the receiver clock by the GD is necessary to remove clock fluctuations, even in the case of a steering clock configuration in the UBLOX receiver.

By subtracting the previous estimations of the clocks and other geodetic terms from the measurements, the residual carrier phase for a given frequency f and a given receiver (rcv) and satellite (sat) pair, $\tilde{L}_{f_{\mathrm{rcv}}}^{\mathrm{sat}}$ in meters, can be represented by the following equation:

$$\tilde{L}_{f_{\mathrm{rcv}}}^{\mathrm{sat}} = -\alpha_f I_{\mathrm{rcv}}^{\mathrm{sat}} + \lambda_f\left(N_f + \delta_{f,\mathrm{rcv}} - \delta_f^{\mathrm{sat}}\right) + \varepsilon_f \tag{3}$$

where λ_f is the wavelength of the GNSS signal; $N_f + \delta_{f,\ \mathrm{rcv}} - \delta_f^{\mathrm{sat}}$ is the carrier phase ambiguity that can be split

Table 1 Receivers used in present study.

Receiver ID	Country	Receiver type (approximate price)	Antenna	Longitude (°)	Latitude (°)
UPC1	Spain	Septentrio MOSAIC-X5 (0.6 k€)	SEPPOLANT_X_MF	2.1	41.4
UPC2	Spain	Septentrio POLARX5E (10 k€)	SEPPOLANT_X_MF	2.1	41.4
UPC3	Spain	UBLOX ZED-F9P (0.2 k€)	SEPPOLANT_X_MF	2.1	41.4
KOS1	Netherlands	Septentrio POLARX5E (10 k€)	LEIAR25.R3	5.8	52.0
DYNG	Greece	Septentrio POLARX5 (10 k€)	TRM59800.00	23.9	37.9

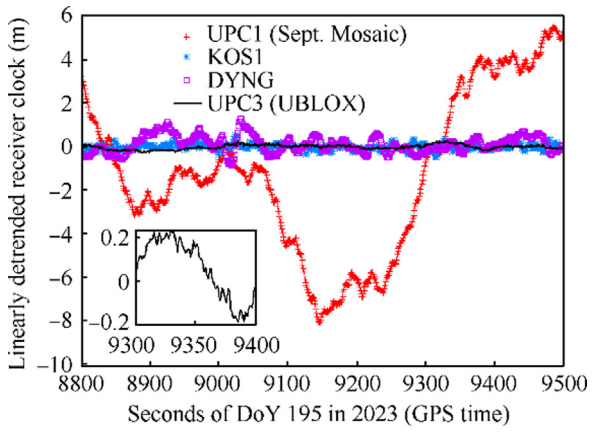

Fig. 1 Example of high-frequency fluctuations of clocks used by different receivers in present study. The zoomed-in graph in the bottom left side illustrates the fluctuations of the UBLOX clock during 100 s.

into an integer part, N_f, plus two real-valued instrumental biases $\delta_{f,\mathrm{rcv}}$ and δ_f^{sat}; and ε_f represents the unmodelled noise of the carrier phase. Finally, $I_{\mathrm{rcv}}^{\mathrm{sat}}$ is the ionospheric delay experienced by the signal, expressed in TEC units (TECU), and α_f is a factor that converts the ionospheric delay from TECU to meters of the given signal identified by the subscript f.

When residuals $\tilde{L}_{f_{\mathrm{rcv}}}^{\mathrm{sat}}$ are not affected by the CSs, the ambiguity term in Eq. (3) remains nearly constant because the variation in instrumental biases is very slow. Therefore, to isolate the true ionospheric fluctuations produced by scintillation, it is essential to detect CSs and identify the continuous arcs of the carrier-phase measurements. To this end, GD proceeds in two steps. First, when geodetic corrections were applied, large discontinuities in the carrier phases were identified, creating separate arcs of the carrier-phase values. Second, from the detrended residuals $\tilde{L}_{f_{\mathrm{rcv}}}^{\mathrm{sat}}$, the IF combination of two carrier phases with different frequencies was used to identify the CSs, which are given by a small integer number of cycles (elemental CSs). Owing to the accurate modelling and corrections previously performed, the fluctuations in the IF combination are typically a few centimetres, which makes it possible to detect jumps, even of a single cycle, in any of the two signals used to build that combination.[10,12] Thus, the methodology applied at this stage of the GD technique can detect whether the CS affects only one or both of the signals used in the IF combination.

Once the different arcs of CS-free continuous carrier phase measurements have been identified, the final component of the GD technique applies an HPF to the detrended measurements. A cut-off frequency of 0.1 Hz is used to remove the remaining low-frequency variations.[11,12] The resulting HPF residuals are then used to calculate the 1-min standard deviations that provide the values of the phase scintillation index, σ_φ, every 60 s for a given carrier phase frequency. The performance of the σ_φ values derived with the GD technique compared to the ISMR outputs has been demonstrated in previous studies.[12,13]

Moreover, because GD requires processing two signals of different frequencies in parallel, an HPF can also be applied to the GF combination, L_{GF}, which is equal to the difference between the two carrier-phase observations. Subsequently, the filtered results can be used to derive the standard deviation in intervals of 1 min, which is henceforth denoted as σ_{GF}.[11] This index measures the ionospheric fluctuations that affect the GF combination of two carrier phases of different frequency,[11] which is used to calculate the ROTI. The HPF residuals of L_{GF} are used to quantify the noise level of that combination and compare it with that of the HPF residuals of the L1 carrier-phase frequency for both low-cost and geodetic receivers.

Finally, to determine the amplitude scintillation index S_4, the GD technique uses the 1 s carrier-to-noise density ratio (C/N_0) recorded in the RINEX files from conventional GNSS receivers to estimate the signal intensity in Eq. (1). This specific procedure has been introduced and subsequently validated in previous studies.[4,13,19] The S_4 calculation uses the 1 min averaging time intervals belonging to the CS-free continuous arcs of carrier-phase residuals obtained after GD processing. The S_4 index derived in this manner has been assessed against the values obtained by collocated ISMRs, and good consistency between the two estimates has been demonstrated.[4,13,19]

3. Experimental setup

3.1. Dataset

Table 1 lists the receivers used to collect the GNSS measurements in this study. The approximate prices of the different receiver models are listed in parentheses in Column 3. Two low-cost mass-market receivers were evaluated in this study: a Septentrio Mosaic-X5 GNSS module installed in a development kit (see https://shop.septentrio.com/en/shop/mosaic-x5-devkit firmware version 4.10.0.1) and a UBLOX ZED-F9P module (https://www.u-blox.com/en/product/zed-f9p-module). Both were connected to a Septentrio SEPPOLANT_X_MF GNSS antenna for data collection. These devices were located in Barcelona, Spain, at the Universitat Politècnica de Catalunya (UPC) premises, and their details are provided in Table l. These two receivers were connected to an ALDCBS1X4-TNC splitter along with a geodetic-grade GNSS receiver, the Septentrio PolarX5E model, designated as UPC2. Therefore, UPC1, UPC2, and UPC3 collect signals from a single antenna located at the same position determined by the common phase centre. Furthermore, it is important to note that the UBLOX receiver has different characteristics compared to the other receivers:

(1) It does not collect global positioning system (GPS) L2W carrier phase measurements, only L2C.
(2) It collects the Galileo E5b signal but not the E5a signal, whereas the other receivers use E5a.
(3) The C/N_0 resolution is 1 dB-Hz, whereas the other receivers have a resolution of 0.1 dB-Hz.

The lower C/N_0 resolution of UBLOX negatively impacted the resulting S_4 index computation in the absence of scintillation, when the lowest values were recorded. For this reason, we decided to exclude the amplitude scintillation index from UBLOX when presenting the results, and we only used the phase scintillation index σ_φ to assess the performance of that receiver in the subsequent comparisons.

Two geodetic receivers belonging to the IGS network were used to collect additional reference data for a comparative analysis. KOS1 is located in the Netherlands, at a similar longitude as the group of receivers in Spain but at a higher latitude. DYNG is situated in Greece at a similar latitude as the receivers in Spain, but at a different longitude. The characteristics of both devices are listed in Table 1. All the devices were located in a mid-latitude region within the European continental area. The approximate cost of the receivers is also shown in Table 1. In addition, the price of the antenna must be considered. The receivers located in Spain share the same antenna manufactured by Septentrio. The cost of this antenna is about 500 €, while in the case of the low latitude receiver mentioned in Section 5, the price of the antenna (JCA228B) is about 120 €.

To analyse the scintillation index S_4 and the standard deviation of the HPF carrier-phase residuals using the proposed methodology, data at a sampling frequency of 1 Hz from the receivers listed in Table 1 were collected over a period of six days, from day of year (DoY) 195 (13th July) to DoY 200 (19th July) in 2023. The motivation for choosing this specific period was to ensure a quiet ionosphere, as no significant level of ionospheric activity was observed. For example, during the aforementioned six-day period, the geomagnetic Kp index was typically less than 4, with only a few time intervals reaching larger values but never exceeding 5. Moreover, no relevant space-weather events were reported during this period, and the ionosphere in the European region showed very little or no activity, as expected for a mid-latitude region during the summer period.

Fig. 2 shows the values of the along arc TEC rate (AATR) indicator for the three locations of the receivers listed in Table 1. The AATR is conventionally used to quantify the ionospheric activity.[20] The results shown in Fig. 2 confirm that the ionosphere was essentially quiet during the experiment period because the 5 min AATR was typically < 0.3 TECU/min during data collection, which corresponds to low-level or no ionospheric activity.[20]

The absence of ionospheric activity at the receiver locations is necessary to characterise the noise level of the scintillation parameters calculated using the GD technique. This noise level is used to establish the minimum threshold for detecting scintillation and allows the determination of the detection capability of low-cost receivers, which is the main objective of this study.

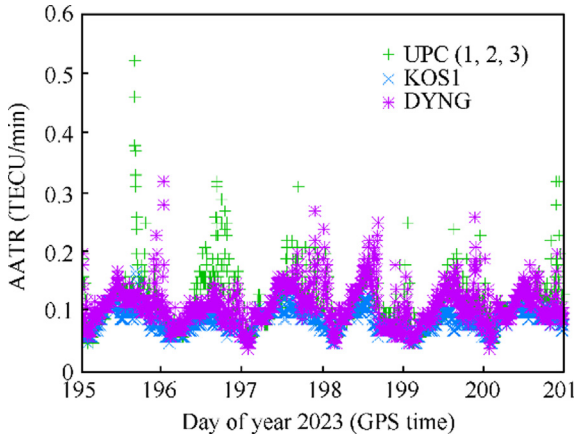

Fig. 2 AATR index calculated over intervals of 300 s in three different locations of receivers used in this study over full analysis period.

For the measurements collected in the present experiment, we considered the carrier phases recorded in the RINEX files of each device for two different signal frequencies transmitted by satellites in the GPS and Galileo constellations. In GPS satellites, the L1 and L2 frequencies have been studied. Moreover, for the L2 band, the P-code-based L2W measurements (RINEX observation code) were collected for all satellites, and when available, code-derived L2C measurements were collected separately. Thus, it was possible to analyse the differences in the GF combination when computed using either L1/L2W or L1/L2C. For the satellites from the European GNSS Galileo, the collected carrier-phase measurements corresponded to the E1 and E5a frequencies. However, as mentioned previously, because the UBLOX device can only collect the pairs of carrier phases L1C/L2C for GPS and E1/E5b for Galileo, only the corresponding GF combinations from those pairs of signals can be considered for the receiver.

Note that the carrier frequencies of L1 and E1 are the same; however, the carrier frequency of E5a is the same as that of GPS L5.

3.2. Checking satellite clocks

The clock offsets from the GPS and Galileo satellites used by the GD method in this study were obtained from the rapid-clock product provided by the German GeoForschungsZentrum (GFZ), an IGS analysis centre. These products are made available in daily files, where values are provided every 30 s throughout the day. Hence, the satellite clocks must be interpolated at 1 s intervals to correct the carrier-phase measurements processed every second using the GD method. Therefore, it is necessary to assess satellite clock fluctuations to verify that the 30 s clocks are sufficiently stable to avoid introducing mismodeling in the interpolated satellite clock corrections. Anomalous fluctuations in satellite clocks produce systematically large values in the phase scintillation index from that satellite at any elevation angle.[12,21] An example of the effect produced by an unstable clock in the values of the σ_φ index is presented in Fig. 3 for the Galileo satellite PRN E19. This satellite belongs to the in-orbit validation (IOV) phase of the Galileo constellation. Fig. 3 shows that the values of σ_φ obtained from satellite E19 for the receivers DYNG (red squares) and KOS1 (green circles) are biased towards larger values compared with the corresponding values from the other Galileo satellites (blue squares). This occurred for the entire period when satellite E19 was in view of the locations of the two IGS receivers in DoY 195 with an elevation greater than 30°. A similar effect was observed for other receivers in the experiment. Because the GD method corrects for satellite clock biases, the large values of σ_φ from a given satellite in regions where no scintillation is expected suggest an anomalous behaviour of the satellite clock.

To verify the previous point, the linearly detrended clock (in meters) for satellite E19 for a full day is shown in Fig. 4. In this figure, the large fluctuations observed in the 30 s clocks from GFZ for Galileo satellites E19 (in red) and E11 (in blue) can be compared with the typical fluctuations of a stable clock illustrated by Galileo satellite E30 (in green). Fig. 4 confirms

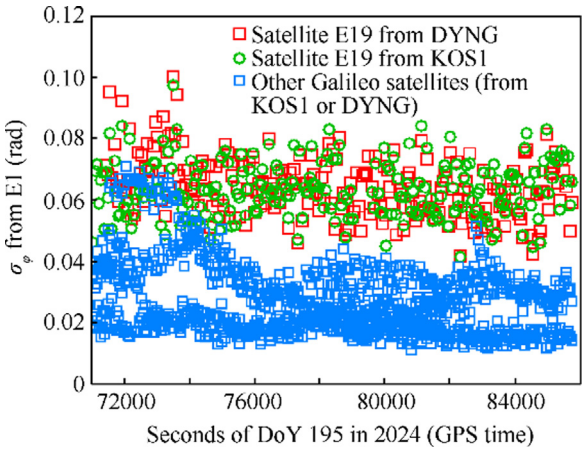

Fig. 3 Comparison between σ_φ index values derived from Galileo satellite E19 for receivers DYNG, KOS1, and from other Galileo satellites.

that the clock of E19 shows high-frequency fluctuations of several centimetres compared to the more stable clock of satellite E30. Moreover, the clock of Galileo satellite E11 is affected by large fluctuations produced by a fast drift in its clock which produces biased values in the σ_φ index. This satellite also belongs to the IOV phase of Galileo. Therefore, satellites E11 and E19 were excluded from the calculation of the HPF carrier-phase residuals analysed in Section 4.2.

Finally, after performing a similar examination of the results from GPS observations, the satellites PRN G05 and G08 were identified to be affected by fast fluctuations in their respective clocks, producing a systematic positive bias in the σ_φ index calculated from their L1 carrier-phase measurements. Fig. 5 illustrates this case, showing an example of the large fluctuations observed in the 30 s clocks from GFZ for GPS satellites G05 and G08 (red and blue symbols, respectively) compared with the typical fluctuations of a stable clock illustrated by GPS satellite G25 (green symbols). The plot in the bottom right is a zoomed-in image of a 1 h interval showing the fluctuations of the clocks in more detail. The clock fluctuations shown by G05 and G08 were substantially larger than those observed in other satellites from the GPS constellation, represented by satellite G25 in Fig. 5. This is confirmed by looking at the smaller graph inserted at the bottom-right of Fig. 5, which clearly shows that, on short timescales, the fluctuations of the clocks in satellites G05 and G08 were significantly larger than those of G25. Consequently, GPS satellites G05 and G08 were excluded from the analysis of the HPF carrier-phase residuals.

4. Results

We present the results in two subsections: one devoted to the S_4 analysis and the other devoted to the HPF carrier-phase residual analysis. The metric used to compare the results from different receivers or GNSS constellations was based on the cumulative distribution function (CDF) derived after integrating the frequency distribution of a given scintillation parameter in different cases and for the total time period considered in this study. Only measurements corresponding to satellite elevations greater than 30° were selected to calculate the different CDFs. To better visualise the largest percentiles of the CDFs, we used the complementary CDF (CCDF), which is equal to one minus the CDF. Consequently, a point (X, Y) of the CCDFs depicted in this section corresponds to a probability Y (expressed in %) of having an S_4 or HPF value greater than X. In particular, the values corresponding to two percentiles, 99% and 99.9%, from the CDFs, or equivalently, 1% and 0.1% probabilities in the CCDFs, respectively, are used to perform a quantitative comparison of the results. The values of these percentiles are indicated in the figures by the intersection points between the black horizontal lines and the different CCDF curves.

4.1. S_4 analysis

Fig. 6 shows the CCDF of S_4 values considering the data from the six-day time period used in this study from the GPS L1 frequency, Fig. 6(a), and Galileo E1 frequency, Fig. 6(b). The results are presented for each of the receivers in Table 1 except for UPC3, which was excluded because of its poor C/N_0 resolution. For the remaining receivers, the distributions of the two constellations were similar. As expected, low S_4 values were

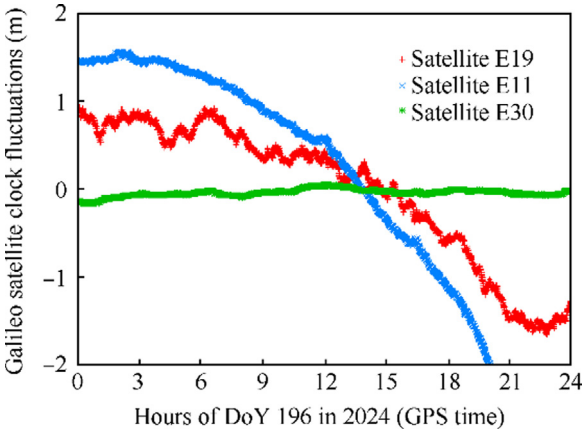

Fig. 4 Linearly detrended Galileo satellite clocks during DoY 196.

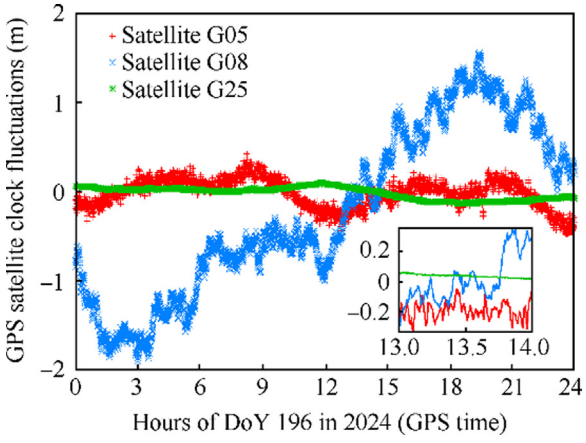

Fig. 5 Linearly detrended GPS satellite clocks during DoY 196 and a zoomed-in graph of interval from 13 to 14 h.

obtained in all the cases, corresponding to a quiet ionosphere. Only some instances with S_4 over 0.2 were observed in less than 0.02% of the cases in the total sample. Consequently, no significant scintillation amplitude was detected.

The two collocated receivers in Barcelona, UPC1 and UPC2, showed nearly identical distributions for both Galileo and GPS, as shown in Fig. 6. The fact that these two devices are connected to the same antenna by means of a splitter may contribute to the similarity in the C/N_0 values and the corresponding signal intensity used to calculate the S_4 index. Regardless, because no significant differences were observed between the collocated receivers, it can be concluded that the low-cost Septentrio Mosaic-X5 (UPC1) had nearly the same performance as the geodetic Septentrio POLARX5E (UPC2) in terms of the measured amplitude scintillation index.

However, Fig. 6 shows that the S_4 values derived from the IGS receivers KOS1 and DYNG are slightly smaller than those in the case of the two collocated receivers UPC1 and UPC2 in Barcelona. These differences can be quantified using the 99th and 99.9th percentiles of the CCDFs presented in Table 2, which are illustrated in Fig. 6 by the intersection of the upper and lower horizontal lines, respectively, with the coloured curves. Table 2 shows that the percentiles from the receivers in Barcelona were larger than those from the IGS receivers. In the case of Galileo, this difference was slightly smaller than that from GPS. However, the observed differences were small. In practice, the minimum threshold to distinguish true amplitude scintillation from residual noise under null scintillation in the case of the Septentrio Mosaic-X5 (UPC1) can be set around 0.15 for GPS (0.13 for Galileo) considering the 99.9th percentiles of the distributions displayed in Fig. 6 (see Table 2). The corresponding threshold for the two Septentrio receivers, KOS1 and DYNG, was nearly 0.1 according to the 99.9th percentiles in Table 2. Consequently, it is possible to use the Septentrio Mosaic-X5 receiver for amplitude scintillation detection and monitoring. The events producing S_4 values greater than a conservative value of 0.2 cannot be attributed to the typical noise of the measurements from that device. Therefore, by using a low-cost Septentrio Mosaic-X5 device connected to a geodetic-grade antenna, such as that used in the present experiment, it is feasible to monitor a wide range of scintillation activities affecting the signal amplitude, ranging from moderate to intense events.[13]

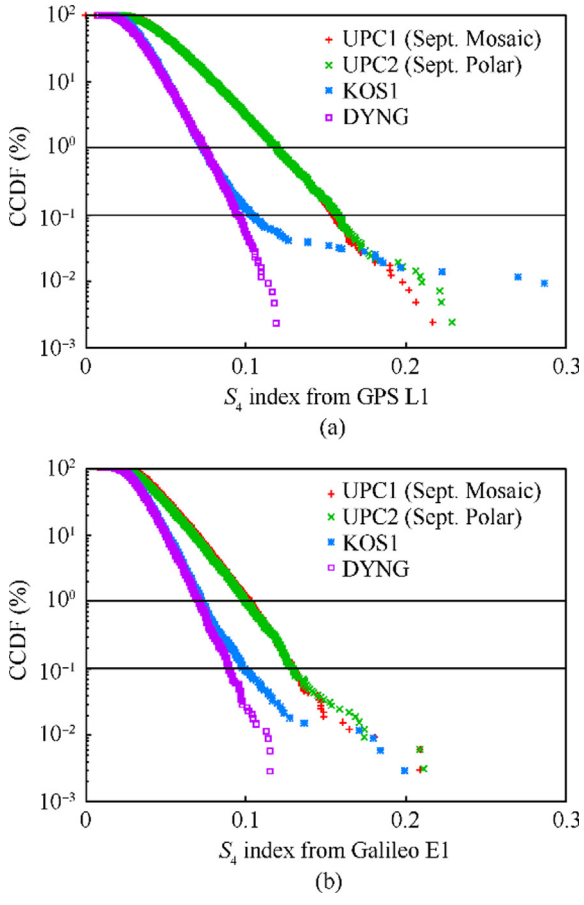

Fig. 6 Distributions of amplitude scintillation index, S_4, for four Septentrio receivers. (a) GPS L1 carrier phase. (b) Galileo E1 carrier phase.

4.2. Analysis of HPF carrier-phase residuals

As previously indicated, the 1 min standard deviation of the HPF residuals from the uncombined L1 or E1 frequency is the classic phase scintillation index, denoted as σ_φ.[12] By contrast, the 1 min standard deviation of the HPF residuals from the GF combinations analysed in the present study considering GPS signals are denoted as $\sigma_{GF}(2W)$ when using L1/L2W and $\sigma_{GF}(2C)$ when using L1/L2C. In the case of the Galileo signals, the 1 min standard deviation of the HPF residuals from the GF combination using E1 and E5a (or E5b in the case of the UBLOX receiver) are indicated by $\sigma_{GF}(5)$.

Fig. 7(a) shows the CCDFs for the occurrence of a given value of σ_φ (red), $\sigma_{GF}(2W)$ (green), and $\sigma_{GF}(2C)$ (blue) for each individual receiver and the GPS constellation. By contrast, Fig. 7(b) shows the corresponding CCDFs of the classic σ_φ index (red) and $\sigma_{GF}(5)$ (blue) obtained from the Galileo signals. The intersection of the black horizontal lines in the graphs with the coloured curves indicates the 99th and 99.9th percentiles of the distributions (upper and lower lines, respectively). Finally, Tables 3 and 4 present the values of these two percentiles for the different CCDFs, as displayed in Fig. 7. To allow a consistent comparison between the results from the different signals, units of TECU were used to express the numerical values in Tables 3 and 4 and on the x-axes of the graphs in Fig. 7. Note that the σ_φ index is typically reported in radians. For this reason, the corresponding percentiles of this index are also expressed in radians in columns 2 and 3 of Tables 3 and 4, where 0.01 TECU is equal to 0.054 rad in the L1/E1 frequency.

Focusing on the results from the GPS satellites, Fig. 7(a) shows a significant difference in the CCDFs derived from the respective indices σ_φ, $\sigma_{GF}(2W)$, and $\sigma_{GF}(2C)$. In principle, the three indicators should measure the same ionospheric fluctuations in TECU, either after GD processing or from the detrending performed by means of the GF combinations, but this was not the case. The ionospheric TEC fluctuations from the HPF residuals of the GF combination using L2W were biased towards smaller values than those from the HPF L1 residuals. This negative bias of the $\sigma_{GF}(2W)$ values from the GF combination that used L1/L2W has been demonstrated to be related with the L1-aided tracking technique

Table 2 99th and 99.9th percentiles of CDF of S_4 index from the L1/E1 frequency for different receivers used in this study.

Receiver	99th Percentile		99.9th Percentile	
	GPS	Galileo	GPS	Galileo
UPC1	0.12	0.10	0.15	0.13
UPC2	0.12	0.10	0.15	0.13
KOS1	0.07	0.07	0.10	0.10
DYNG	0.07	0.07	0.10	0.09

implemented in the Septentrio receivers, which is used to recover the GPS L2W carrier-phase observation.[22] This tracking procedure introduces a correlation between L2W and L1, producing smaller values of the HPF residuals from the GF combination that uses L1/L2W measurements.[11] All the analysed Septentrio receivers (both low-cost and geodetic) were similarly affected by the negative bias in the $\sigma_{GF}(2W)$ compared to the σ_φ distributions of the L1 HPF residuals, as shown in Fig. 7(a), green symbols.

Concerning the CCDF of the $\sigma_{GF}(2C)$ values, the results displayed in Fig. 7(a) (red symbols) clearly show a positive bias with regard to the σ_φ distribution from L1 in all the analysed receivers (Septentrio and UBLOX). Considering the absence of ionospheric activity during the analysis period, the distributions of σ_φ values should only be affected by the residual error in the detrended L1 carrier phase, which results from measurement noise and the mismodelling errors introduced by the GD processing. However, the effects of these errors in the σ_φ index were smaller than those resulting from combining measurements at the L1 and L2 frequencies. Moreover, when calculating the GF combination of L1/L2C assuming uncorrelated signals, an increase in the error of this combination concerning the error from each individual signal should result because the errors from the two combined signals are added. The resulting noise of the $\sigma_{GF}(2C)$ index is typically larger than that affecting the σ_φ index from the uncombined L1 measurements, which is reflected in the distributions depicted in Fig. 7(a) (blue and red symbols) and in the percentile values shown in Table 3. The same conclusion was obtained for the Galileo data when comparing the CCDF of the σ_φ index from the uncombined E1 measurements (red curves in Fig. 7(b)) with the distribution of $\sigma_{GF}(5)$ from the GF combination using L1/E5a for the Septentrio receivers and E1/E5b for the UBLOX receiver (blue curves in Fig. 7(b)). Here, the error increase affecting the $\sigma_{GF}(5)$ index concerning σ_φ could be quantified using the percentile values displayed in Table 4.

Finally, a quantitative comparison of the percentiles presented in Tables 3 and 4 for GPS and Galileo, respectively, shows that the CCDF of the σ_φ index from the low-cost receiver UPC1 was very similar to that obtained using the geodetic-grade receivers for the two GNSS constellations. In all cases, the value of the 99.9th percentile of the distribution of the σ_φ index was approximately 0.06 rad for GPS, and only slightly lower (~0.05 rad) for Galileo. In the case of the UBLOX receiver (UPC3), although the percentiles of the σ_φ index were slightly higher than those of the other Septentrio receivers, they were smaller than the percentiles obtained using the GF combinations from that receiver. Nevertheless, the magnitude of the UPC3 percentiles can be considered to be at the same level as that of the geodetic receivers. This implies that, for all the devices included the low-cost receivers UPC1 and UPC3 and for the two constellations, a common value can be assumed for the minimum threshold of the σ_φ index to distinguish scintillation activity from quiet periods. Conservatively, this common value could be set to 0.1 rad, which is sufficient to monitor most scintillation events that produce significant carrier phase fluctuations in L1/E1 carrier frequency measurements.[13] Therefore, the Septentrio Mosaic X5 and UBLOX ZED-F9P receivers can distinguish phase scintillation events showing a σ_φ index > 0.1 rad from the lower values associated with residual noise produced during quiet periods without scintillation, in the same manner as the geodetic receivers.

5. Case study of a low-cost receiver under scintillation

In the previous section, we conducted our study using data collected under non-scintillation conditions. Because the GD technique corrects observations for all effects that can be confused with ionospheric scintillation, only the ionospheric scintillation and thermal noise remain after applying the HPF. Therefore, by analysing the data without scintillation, the thermal noise specific to each receiver can be characterized and thresholds for the detection of actual scintillation can be established. As shown in the previous section, low-cost receivers have only a slightly higher thermal noise than geodetic receivers. The values of σ_φ from low-cost receivers can then be considered to be at the same level as the values obtained using geodetic receivers.

However, it is unclear whether this conclusion holds under scintillation conditions. To address this issue, we considered data from an additional receiver, A010 (located in Peru; 77°W, 12°S), equipped with the same UBLOX system as UPC3 and connected to a JCA228B antenna (approximate price 120 €). Unfortunately, we only had access to data from A010 for a limited number of days in 2024; therefore, we selected a six-day period, similar to the other five receivers presented in Table 1. The analysis period began on DoY 72 of 2024, from 12 to 17 March. It should be noted that the analysis of data from A010 is provided as an example to further illustrate the performance of a low-cost receiver affected by scintillation as a detailed study of scintillation activity based on low-cost receivers is beyond the scope of the present study.

Fig. 8 shows the σ_φ time series for the two UBLOX receivers A010 and UPC3 during the corresponding six-day periods. The results from the Galileo and GPS satellites are similar, so only the values from GPS are shown in Fig. 8. As expected, after local sunset, the low-latitude receiver A010 experiences phase-scintillation episodes close to 0.1 TECU in L1 (0.54 rad), a large value for a low-latitude receiver, similar to the one achieved by some receivers located at high latitudes.[13] By contrast, σ_φ values for UPC3 are clearly lower than 0.02 TECU (0.1 rad), indicating the absence of scintillation, and the resulting σ_φ can be attributed to thermal noise.

This latter result is illustrated by the CCDF curves displayed in Fig. 9, where in up to 90% of cases, σ_φ was < 0.01 TECU, corresponding to periods without scintillation, and the distributions from the two receivers overlap. However, approximately 10% of the σ_φ values reported by

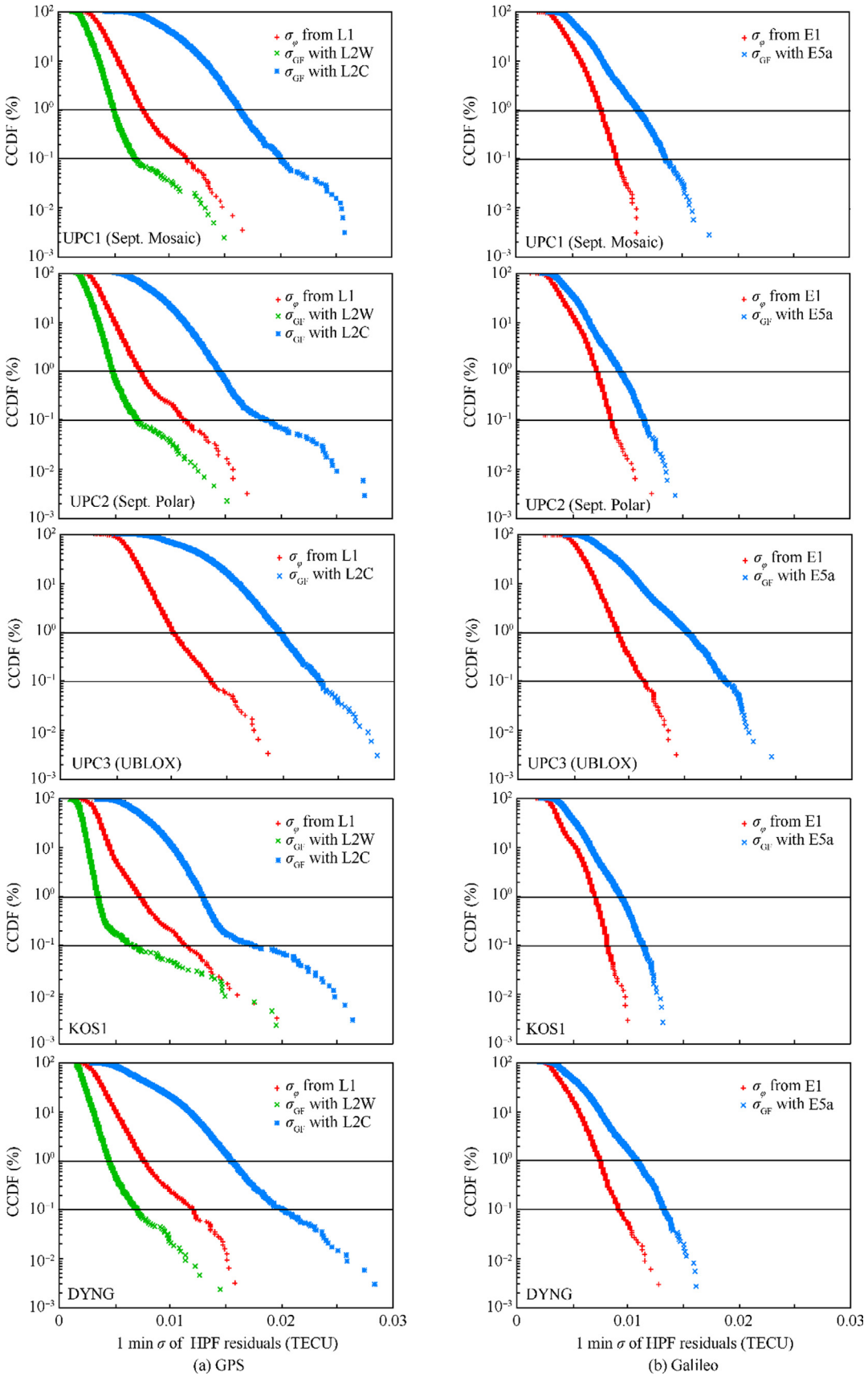

Fig. 7 CCDF of the 1 min standard deviation of HPF carrier-phase residuals. Measurements were collected during the six days analysed in 2023 by the five receivers analysed. The curves were obtained from L1 or E1 after applying GD (red), the GF combination of L1 and L2W (green), and the GF combination of L1 and L2C for GPS or E1 and E5a (E5b in the case of UPC3 UBLOX) for Galileo (blue).

Table 3 Summary of the 99th and 99.9th percentiles (in TECUs) for the GPS satellites from the CCDFs of 1 min σ values derived from different HPF residuals of the five analysed receivers. In the case of σ_φ from L1, the corresponding radian values are provided in parentheses.

Receiver	σ_φ(uncombined L1)		σ_{GF}(2C)(GF comb. with L2C)		σ_{GF}(2W)(GF comb. with L2W)	
	99th percentile	99.9th percentile	99th percentile	99.9th percentile	99th percentile	99.9th percentile
UPC1	0.008 (0.043 rad)	0.011 (0.06 rad)	0.016	0.020	0.005	0.007
UPC2	0.007 (0.038 rad)	0.011 (0.06 rad)	0.014	0.019	0.005	0.007
UPC3	0.010 (0.054 rad)	0.013 (0.07 rad)	0.020	0.023		
KOS1	0.007 (0.038 rad)	0.011 (0.06 rad)	0.013	0.017	0.003	0.007
DYNG	0.008 (0.043 rad)	0.012 (0.065 rad)	0.015	0.020	0.004	0.007

Table 4 Summary of the 99th and 99.9th percentiles (in TECUs) for the Galileo satellites from the CCDFs of 1 min σ values derived from different HPF residuals of the five analysed receivers. In the case of σ_φ from L1, the corresponding radian values are provided in parentheses.

Receiver	σ_φ(uncombined E1)		σ_{GF}(5)(GF comb. with E5a/E5b)	
	99th percentile	99.9th percentile	99th percentile	99.9th percentile
UPC1	0.008 (0.043 rad)	0.009 (0.049 rad)	0.011	0.014
UPC2	0.007 (0.038 rad)	0.0085 (0.046 rad)	0.009	0.012
UPC3	0.009 (0.049 rad)	0.011 (0.06 rad)	0.015	0.019
KOS1	0.007 (0.038 rad)	0.008 (0.043 rad)	0.009	0.0115
DYNG	0.008 (0.043 rad)	0.009 (0.049 rad)	0.011	0.013

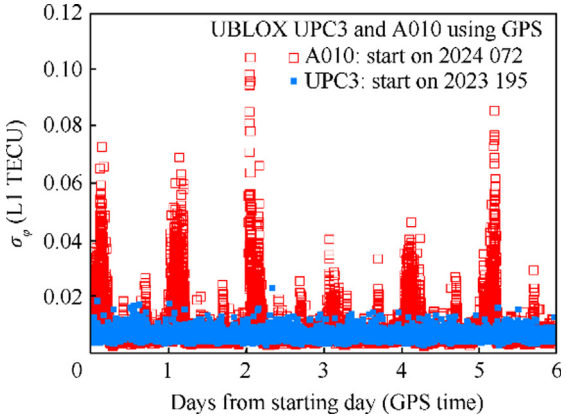

Fig. 8 Time series of the phase scintillation index σ_φ over a continuous six-day period. Red: the low-latitude receiver A010 data starting on DoY 72 of 2024. Blue: the mid-latitude receiver UPC3 data starting on DoY 195 of 2023.

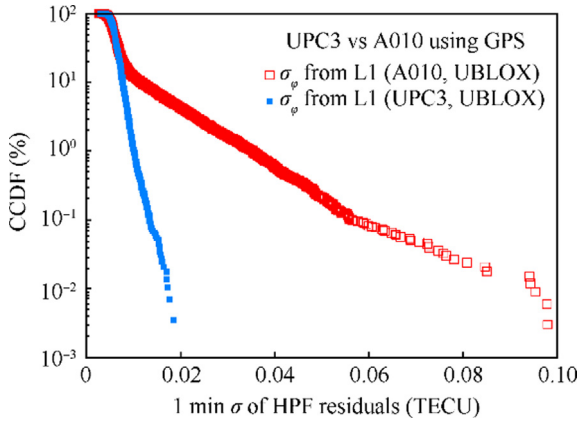

Fig. 9 Two CCDF plots of σ_φ corresponding to respective time series of values shown in Fig. 8.

A010 were greater than 0.015 TECU and corresponded to scintillation episodes. Some of these values were quite intense, as indicated by the long tail in the CCDF plot, which is not present in the distribution from UPC3. These results illustrate that a low-cost receiver such as UBLOX is capable of detecting scintillation events as they occur, demonstrating its feasibility for scintillation monitoring.

6. Conclusions

(1) A feasibility study based on the GD technique was performed to analyse the minimum resolution required to perform scintillation monitoring using several receivers connected to geodetic-grade antennas. The results demonstrated that the low-cost receivers Septentrio Mosaic X5 and UBLOX ZED-F9P showed similar performances to the geodetic receivers manufactured by

Septentrio that were located in permanent ground-monitoring stations in the IGS network. Geodetic receivers are typically ten to 50 times more expensive than low-cost receivers. This implies the possibility of achieving global scintillation monitoring using low-cost receivers in areas of poor coverage, thereby reducing costs and increasing the density of ground receivers for the local detection and characterisation of ionospheric fluctuations produced by scintillation.

(2) Based on the data collected for six days during a period of null scintillation, minimum thresholds to identify scintillation activity with the GD method were determined for the S_4 and σ_φ indices derived from observations of the L1 and E1 frequencies. Considering the amplitude scintillation index, S_4, obtained using the Septentrio Mosaic X5 device, threshold values of approximately 0.15 and 0.13 can be applied to the GPS L1 and Galileo E1 signals, respectively. These values were only slightly higher than 0.1, which was the value obtained for the two IGS geodetic receivers that were analysed. In the case of UBLOX ZED-F9P, the poor resolution of the carrier-to-noise density ratio prevented analysis of the S_4 index. Conversely, for the phase scintillation index, σ_φ, a common minimum threshold for scintillation detection of $\sim$ 0.1 rad can be set for both the Septentrio Mosaic X5 and UBLOX ZED-F9P receivers.

(3) Using a second signal to perform a detrending of carrier phases via GF combination produces inconsistencies in the values of the standard deviation of HPF carrier phase residuals when using the GPS L2 signal, which depend on the channel or code that is used (L2C or L2W). Additionally, for the GPS and Galileo measurements, the GF combinations of L1/L2C and E1/E5a signals (E1/E5b in the case of UBLOX), respectively, showed a bias towards larger values considering the uncombined L1 and E1 results. Consequently, the use of uncombined carrier frequencies provides an improved performance, and more consistent results can be achieved for scintillation monitoring than via the GF combination of dual-frequency signals.

(4) Finally, an additional UBLOX receiver was evaluated in a low-latitude region over a six-day period during which post-sunset scintillation episodes characteristic of that region were effectively detected. This experiment further illustrated the feasibility of using low-cost receivers for scintillation monitoring.

We conclude that the low-cost Septentrio Mosaic X5 and UBLOX ZED-F9P devices show sufficient resolution for scintillation monitoring using the GD method based on the uncombined GPS L1 or Galileo E1 frequencies.

CRediT authorship contribution statement

Guillermo GONZÁLEZ-CASADO: Writing – review & editing, Writing – original draft, Methodology, Conceptualization. **Jorge GARCÍA-MATEOS:** Validation, Software, Formal analysis. **Yu YIN:** Writing – review & editing, Writing – original draft, Methodology, Conceptualization. **Angela ARAGON-ANGEL:** Writing – original draft, Methodology, Formal analysis, Conceptualization. **José Miguel JUAN:** Methodology, Conceptualization. **Cristhian C. TIMOTE:** Software, Formal analysis. **Adria ROVIRA-GARCIA:** Writing – review & editing, Validation, Formal analysis. **Jaume SANZ:** Writing – review & editing, Validation.

Declaration of competing interest

The authors declare that they have no known competing financial interests or personal relationships that could have appeared to influence the work reported in this paper.

Acknowledgements

This study has received funding from European Union (MCIN/AEI/10.13039/501100011033/FEDER) (Nos. PID2022-138485OB-I00 and CNS2022-135383) and by European Space Agency (RT-WMIS) (No. 4000137762/22/NL/GLC/ov). Yu YIN had funding support from the China Scholarship Council (No. 202006020025).

References

1. Pi X, Iijima BA, Lu W. Effects of ionospheric scintillation on GNSS-based positioning. *NavigationJ Inst Navig* 2017;**64**(1):3–22.
2. Koulouri A, Smith ND, Vani BC, et al. Methodology to estimate ionospheric scintillation risk maps and their contribution to position dilution of precision on the ground. *J Geod* 2020;**94**(2):22.
3. Aquino M, Dodson AH, Ward P. Ionospheric scintillation effects on GPS positioning. *J Geophys Res: Space Phys* 2009;**114**(A2):A02310.
4. Juan JM, Sanz J, González-Casado G, et al. Feasibility of precise navigation in high and low latitude regions under scintillation conditions. *J Space Weather Space Clim* 2018;**8**:A05.
5. Dierendonck AJV, Klobuchar J, Hua Q. Ionospheric scintillation monitoring using commercial single frequency C/A code receivers. *Proceedings of ION GPS 1993*. Institute of Navigation; 1993.
6. Linty N, Dovis F. An open-loop receiver architecture for monitoring of ionospheric scintillations by means of GNSS signals. *Appl Sci* 2019;**9**(12):2482.
7. Briggs BH, Parkin IA. On the variation of radio star and satellite scintillations with zenith angle. *J Atmos Terr Phys* 1963;**25**(6):339–66.
8. Yeh KC, Liu CH. Radio wave scintillations in the ionosphere. *Proc IEEE* 1982;**70**(4):324–60.
9. Rino CL. A power law phase screen model for ionospheric scintillation: 1. Weak scatter. *Radio Sci* 1979;**14**(6):1135–45.
10. Juan JM, Aragon-Angel A, Sanz J, et al. A method for scintillation characterization using geodetic receivers operating at 1Hz. *J Geod* 2017;**91**(11):1383–97.
11. Juan JM, Sanz J, González-Casado G, et al. Applying the geodetic detrending technique for investigating the consistency of GPS L2P(Y) in several receivers. *J Geod* 2022;**96**(11):85.
12. Nguyen VK, Rovira-Garcia A, Juan JM, et al. Measuring phase scintillation at different frequencies with conventional GNSS receivers operating at 1Hz. *J Geod* 2019;**93**(10):1985–2001.
13. Rovira-Garcia A, González-Casado G, Juan JM, et al. Climatology of high and low latitude scintillation in the last solar cycle by means of the geodetic detrending technique. *Proceedings of the 2020 international technical meeting of the institute of navigation*. Institute of Navigation; 2020.

14. Curone D, Savarese G, Antonini M, et al. An innovative low-power, low-cost, multi-constellation geodetic-grade global navigation satellite system reference station for the densification of permanent networks: the GREAT project. *Sensors* 2023;**23**(13):6032.
15. Vidal M, Jarrin P, Rolland L, et al. Cost-efficient multi-GNSS station with real-time transmission for geodynamics applications. *Remote Sens* 2024;**16**(6):991.
16. Pi X, Mannucci AJ, Lindqwister UJ, et al. Monitoring of global ionospheric irregularities using the Worldwide GPS Network. *Geophys Res Lett* 1997;**24**(18):2283–6.
17. Liu ZZ, Yang Z, Xu DY, et al. On inconsistent ROTI derived from multiconstellation GNSS measurements of globally distributed GNSS receivers for ionospheric irregularities characterization. *Radio Sci* 2019;**54**(3):215–32.
18. Sanz J, Juan JM, Hernández-Pajares M. *GNSS data processing, Vol. I: Fundamentals and algorithms. Noordwijk: ESA Commun* 2013:95–138.
19. Luo XM, Gu SF, Lou YD, et al. Amplitude scintillation index derived from C/N0 measurements released by common geodetic GNSS receivers operating at 1Hz. *J Geod* 2020;**94**(2):27.
20. Juan JM, Sanz J, Rovira-Garcia A, et al. AATR an ionospheric activity indicator specifically based on GNSS measurements. *J Space Weather Space Clim* 2018;**8**:A14.
21. Benton CJ, Mitchell CN. Further observations of GPS satellite oscillator anomalies mimicking ionospheric phase scintillation. *GPS Solut* 2014;**18**(3):387–91.
22. McCaffrey AM, Jayachandran PT, Langley RB, et al. On the accuracy of the GPS L2 observable for ionospheric monitoring. *GPS Solut* 2017;**22**(1):23.